Journal of Power Sources 195 (2010) 3631–3635

Contents lists available at ScienceDirect

Journal of Power Sources

journal homepage: www.elsevier.com/locate/jpowsour

Short communication

Creep properties of solid oxide fuel cell glass–ceramic seal G18

Jacqueline Milhans[a,*], Mohammed Khaleel[b], Xin Sun[b], Mehran Tehrani[c], Marwan Al-Haik[c], H. Garmestani[a]

[a] Georgia Institute of Technology, School of Material Science and Engineering, United States
[b] Pacific Northwest National Lab, United States
[c] University of New Mexico, Department of Mechanical Engineering, United States

ARTICLE INFO

Article history:
Received 27 October 2009
Received in revised form
10 December 2009
Accepted 10 December 2009
Available online 16 December 2009

Keywords:
SOFC
Elastic properties
Creep
Glass–ceramic
Seal
Nanoindentation

ABSTRACT

This study utilizes nanoindentation to investigate and measure creep properties of a barium calcium alumino-silicate glass–ceramic used for solid oxide fuel cell seals (SOFCs). Samples of the glass–ceramic seal material were aged for 5, 50, and 100 h to obtain different degrees of crystallinity. Instrumented nanoindentation was performed on the samples with different aging times at different temperatures to investigate the strain rate sensitivity during inelastic deformation. The temperature dependent behavior is important since SOFCs operate at high temperatures (800–1000 °C). Results show that the samples with higher crystallinity were more resistant to creep, and the creep compliance tended to decrease with increasing temperature, especially with further aged samples.

1. Introduction

Solid oxide fuel cell (SOFC) technology has been demonstrated as a promising and efficient alternative energy source. In planar SOFCs, a hermetic seal is required to separate fuel and air sides of the electrodes. The seal also is often used to bond components of the fuel cell together. This seal must be able to withstand the thermal cycling caused by powering up and powering down the fuel cell, which operates at approximately 800 °C. Also, it is important that the joining temperature of the seal is above the operating temperature of the fuel cell it is intended for. Glass–ceramic materials are currently being investigated as candidates for SOFC sealant materials. This is due to their ability in maintaining mechanical properties at high temperatures, manufacturability and low cost. The seal is bonded to several components of the seal (e.g. interconnect, electrodes, frame, etc.), therefore making it costly to replace. Seal materials must have long life spans due to their difficulty to repair [1–5].

Furthermore, a SOFC seal must not display significant creep at high temperatures to maintain the stack level geometric stability. By understanding the creep properties, the life of the seal may be predicted in terms of creep deformation. In the case of glass–ceramics, changing the degree of crystallinity of the material can alter the properties. The desired level of crystallinity can be produced by a combination of aging time and temperature. The creep properties can be changed to an extent by "designing" the microstructure in this sense of crystalline volume fraction.

In this study, nanoindentation is performed on G18 (a glass–ceramic seal developed by Pacific Northwest National Laboratory [3–8] to determine its temperature- and time-dependent viscoplastic properties. Nanoindentation has been used in other studies, for glasses at high temperatures and more especially for polymers, in finding creep properties [9–14]. Because G18 is a glass–ceramic designed for high-temperature operation, it displays similar viscoplastic characteristics as polymers at high temperatures. Nanoindentation is an effective technique to study mechanical properties high-temperature SOFC materials. High-temperature nanoindentation is used establish mechanical behavior–microstructure relationships in the SOFC seal material. Glass–ceramic seals are multi-phase materials, with the ability to tailor the mechanical behavior through controlling the amount of crystallinity. With better mechanical property–microstructure relationships, development of glass–ceramic seals could be more rapid and progressive. Nanoindentation can also reveal periodicity in mechanical properties, which may be due to phase clustering or other morphologies in the microstructure. Nanoindentation of

* Corresponding author at: Georgia Institute of Technology, 771 Ferst Dr., Love Bldg, Rm 353, Atlanta, GA 30332, United States. Tel.: +1 978 870 7944; fax: +1 404 894 9140.
E-mail address: jackie.milhans@gmail.com (J. Milhans).

0378-7753/$ – see front matter © 2009 Elsevier B.V. All rights reserved.
doi:10.1016/j.jpowsour.2009.12.038

samples with different levels of crystallinity can show the effects of crystalline volume fraction.

In this study, nanoindentation is performed to measure the elastic modulus, hardness, and creep of G18. The tests are performed at different temperatures, up to 400 °C, using Berkovich tip. During nanocreep testing, the indenter is held at the maximum load for a certain period of time. This results in material creep following indentation, which is dependent on the load and holding time. The short time nanocreep tests will in turn help us understand the creep and mechanical behavior of G18.

It is desired to be able to predict the creep behavior at operating temperatures over long periods of time. Nonlinear curve fitting will later be employed in order to predict long-term time-dependent behavior [2,8,15,16]. In this paper, we report the creep experiments and the data measured for G18.

2. Procedure

2.1. Materials and processing

G18 is a barium alumino-silicate (BCAS)-based glass–ceramic at the Pacific Northwest National Laboratory (PNNL) for potential application as a seal material for SOFCs. In addition to providing a hermetic seal over long periods of SOFC operation time, G18 must also help maintain stack geometric stability to minimize creep induced narrowing of the air and fuel flow channels. All these mandate a better characterization and understanding of the G18 creep properties over time and at elevated temperatures. After sintering, a crystallization volume fraction of approximately 55% has been observed. Further aging has shown increases in crystallinity of up to 72% [5,17–19]. The glass transition temperature has been reported as 619 °C and a softening temperature of 685 °C.

The crystalline phases in G18 are needles that are approximately 5–6 μm in length and about 1–3 μm in diameter. As the nanoindenter comes in contact with the sample, the contact area is larger than a micron. Therefore, it is assumed that the indentations cover both the glass matrix and crystalline needle phases because the exact location of the indent is unknown *a priori*.

G18 disks were sintered at 850 °C, and aged at 750 °C for 5, 50 and 100 h. The purpose of the different aging times is to provide different amounts of crystallization in each sample. Sealants aged to maximum crystallinity, such as the 100 h aged sample, will not age further at operating temperature. The purpose of the different aging times is to purely to provide different amounts of crystallization in each sample, which can be done because the tests are below T_g. The samples were then ground and polished to a mirror finish for nanoindentation preparation. Sample damage in the hard, brittle sample is minimal during polishing. If there is damage to the surface or voids within the sample, nanoindentation will show either steps in the indentation curve, or a different surface contact depth than indicated.

2.2. Nanoindentation

Nanoindentation was performed using a Berkovich indenter tip, a three sided pyramid, diamond tip. The indentation was performed on each sample at the temperatures: 25, 200, 300, and 400 °C. Nanoindentation above 400 °C is not yet possible, and therefore, the study was done to understand intermediate SOFC temperatures, such as when they are heating up or cooling down. Indentation tests at higher temperatures will be performed, once the facilities are available. These results are considered as global results, and not results of individual phases. A loading/unloading rate of 2 mN s^{-1} with a maximum load of 50 mN was used to measure the hardness, elastic modulus, and creep properties.

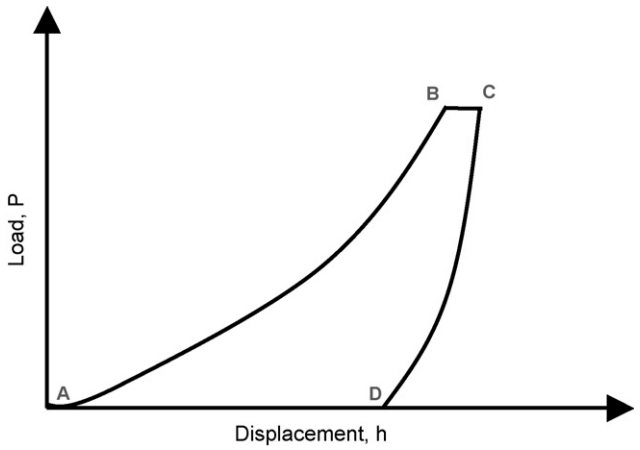

Fig. 1. Load–displacement curve of nanoindentation showing loading, load holding, and unloading.

In order to obtain creep data, the maximum load was held constant for 60 s during each indent before unloading. The dwell data was recorded for the maximum load allowed for the corresponding loading rate. For each thermal condition and sample, 5–10 indents were performed, with a 20 μm spacing. Only individual tests were selected for reporting creep data. This is because it is difficult to average nanoindentation creep data, due to load overshoots by the machine, causing a slight difference maximum load in each test, on the order of 0.1–1 mN. Therefore, the general trend is studied, and a representative test trial of all of the tests is selected. This is within common practice of nanoindentation. The nanoindentation was performed at the University of New Mexico, using a Nano Test system from Micro Materials, Ltd., UK.

2.3. Indentation analysis

When using sharp indentation, for any elastic–plastic material, the loading curve can be described with the following power law:

$$P = Ch^2 \tag{1}$$

where C is a material dependent constant, P is the load, and h is the indentation depth.

The modulus and hardness were calculated using the well-known Oliver–Pharr method [20,21] from the load–displacement curves. A typical indentation curve is shown in Fig. 1 from A to B, the indentation is loading, B to C shows a constant hold for the load, and C to D displays unloading.

Several parameters are needed for calculating the modulus and hardness using the Oliver–Pharr method. The unloading curve, as shown in Fig. 1 can be described by the Oliver–Pharr method as:

$$P = A(h - h_f)^m \tag{2}$$

where A and m are material constants [20,21]. Depth of the indentation, h, is acquired from the indentation, where h_c is the contact depth, h_s is the displacement at the perimeter of the indent. Contact depth and total depth are defined by:

$$h_c = \varepsilon \frac{P_{\max}}{S} \tag{3}$$

$$h_{\max} = h_c + h_s \tag{4}$$

$P_{\max}$ represents the maximum load, which corresponds to the depth $h_{\max}$. At this point, the stiffness is the initial unloading stiffness, S_{pmax}. The correction factor, $\varepsilon = 1.0$ for a spherical tip, and 0.75 for a Berkovich tip.

These parameters can be seen in Fig. 2. The area of contact is calculated as a function of the contact depth, shown below for a

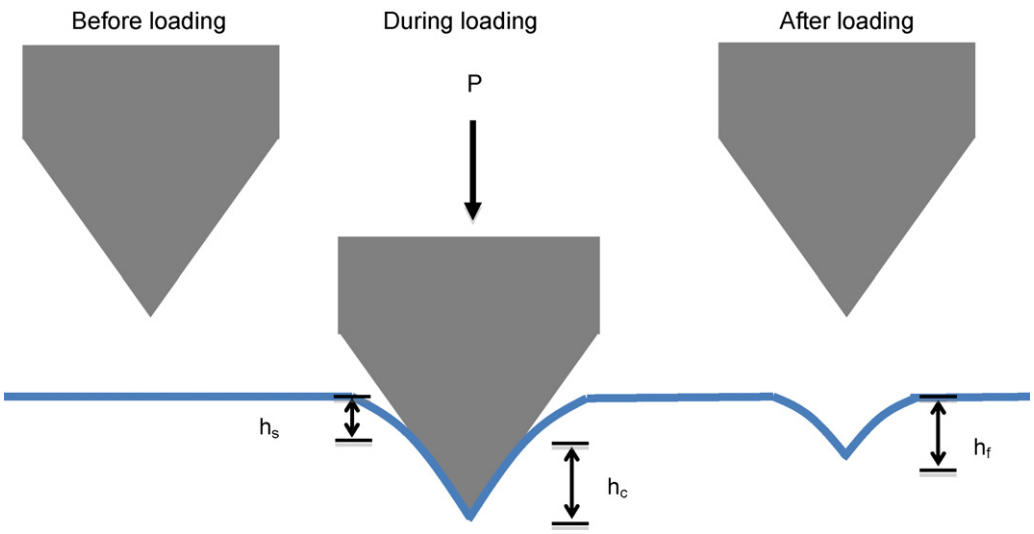

Fig. 2. Scheme of indentation before, during, and after loading.

Berkovich indenter tip:

$$A_c = 3\sqrt{3h_c^2}\,\tan^2 65.3 = 24.5h_c^2 \tag{5}$$

The reduced modulus is given by:

$$\frac{1}{E_r} = \frac{1-\nu_i^2}{E_i} + \frac{1-\nu_s^2}{E_s} \tag{6}$$

where ν is the Poisson's ratio, E is the elastic modulus, and i and s represent the indenter tip and specimen (where for the diamond tip, $\nu_i = 0.07$ and $E_i = 1141$ GPa). The stiffness is related to the load, depth, contact area, and reduced modulus by the following relation:

$$S = \frac{dP}{dh} = 2E_r\frac{\sqrt{A_c}}{\sqrt{\pi}} \tag{7}$$

Also, hardness was calculated, with the contact depth calculated at $h = h_{max}$, using the relationship:

$$H = \frac{P_{max}}{24.5h_c^2} \tag{8}$$

Finally, the elastic modulus of the sample can be calculated from the equation give by:

$$E_s = \frac{dP}{dh}\frac{1}{2h_c}\frac{1}{\beta}\sqrt{\frac{\pi}{24.5}} \tag{9}$$

β is a tip parameter, is 1.034 for a Berkovich indenter tip.

3. Results and discussion

3.1. Hardness and Young's modulus

Using the Oliver–Pharr method, hardness and Young's modulus results are calculated, and shown, in Table 1.

The nanoindentation results in Fig. 3 show that the elastic modulus increases slightly with raised temperature. From 300 to 400 °C, there is a significant jump of about 100% in the elastic modulus. Although previous tests have shown a jump in elastic modulus at 400 °C, the increase is much larger than previous observed [6]. This may be due to self-healing of cracks or some other changes in the microstructure. This should be further examined by high-temperature image analysis.

The hardness stays almost constant, and then, similar to the elastic modulus, almost doubles at 400 °C for each sample. This can be seen in Fig. 4.

Table 1
Hardness and Young's modulus results from indentation.

Sample	Hardness (GPa)	Young's modulus (GPa)
RT 5 h	4.07 ± 1.13	70.33 ± 5.96
RT 50 h	3.90 ± 0.22	66.66 ± 1.21
RT 100 h	3.21 ± 0.88	68.09 ± 5.28
200 °C 5 h	5.42 ± 0.49	78.25 ± 6.44
200 °C 50 h	4.14 ± 0.94	77.11 ± 4.64
200 °C 100 h	3.98 ± 0.64	71.38 ± 2.29
300 °C 5 h	5.32 ± 0.66	80.50 ± 5.99
300 °C 50 h	3.68 ± 0.49	76.40 ± 5.67
300 °C 100 h	3.74 ± 0.84	75.72 ± 4.28
400 °C 5 h	7.47 ± 0.83	121.59 ± 6.42
400 °C 50 h	6.16 ± 0.79	168.52 ± 6.22
400 °C 100 h	8.19 ± 0.80	187.87 ± 6.32

The change in elastic modulus seems to be more affected by the aging time, whereas the hardness seems to be less sensitive to aging at lower temperatures.

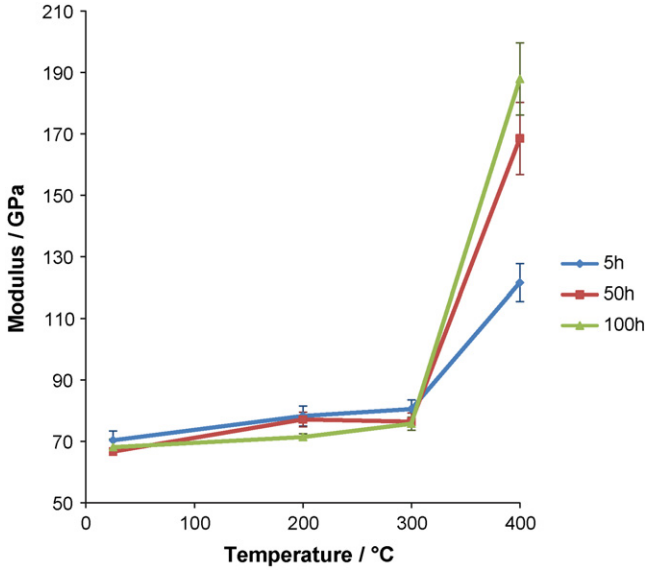

Fig. 3. Reduced modulus results of G18 with different aging times, indented at 750 °C.

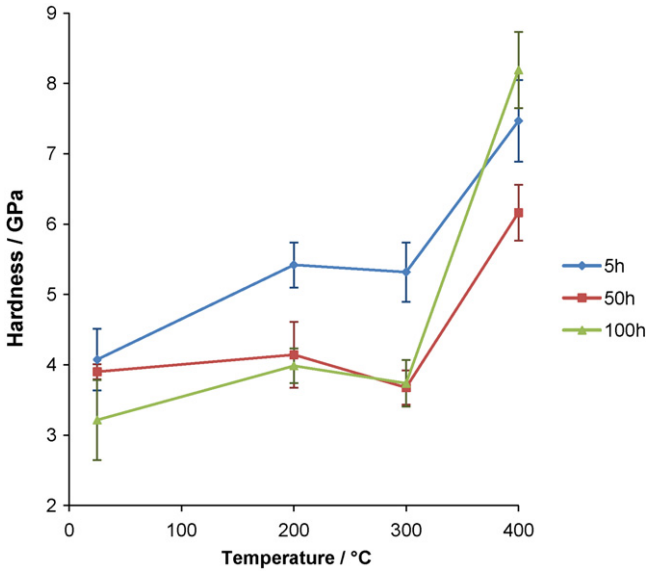

Fig. 4. Hardness results from nanoindentation of different aging times.

3.2. Creep testing

Creep data was normalized, by subtracting the initial depth of each creep test. This is to better compare only the creep results, without taking the depth from the indenting period into consideration.

Samples aged longer did not have such a drastic increase in depth before it reached steady-state creep (the linear portion of the curve). Therefore, samples that were higher in crystallinity were more resistant to creep at high temperatures.

Tests done at lower temperatures reached steady-state creep faster, and were more resistant to creep. This is conclusive from a more linear creep curve, with a small primary creep region. It can be seen that a logarithmic curve is formed during the constant load tests in Fig. 5. There is no drastic creep observed, which is excellent for SOFC performance. The amount of creep does not change significantly with temperature.

3.3. Steady-state creep

The steady-state region of creep is also known as secondary creep. Steady-state regions of curves shown in part B were taken. In order to isolate the steady-state region, the first 20 s of the creep test were removed. This is the portion of the curve where the creep achieves almost linear behavior after its initial primary creep, due to a balance between work hardening and recovery. The linear regression models were obtained by a least-squared approach. The behavior of steady-state creep, with a minimum, constant creep rate, allows for prediction of failure before tertiary creep.

Steady-state creep results as shown in Fig. 6, show that there is no clear dependence on aging time in each temperature range. Comparing across aging time, results show no apparent trend. This is most likely due to the fact that there is no change in behavior at lower temperatures due to aging, below T_g. There is no phase change, or viscoelasticity provided by the glassy phase, and therefore stays a completely brittle material. In order to find the effects of change in microstructure, tests must be repeated at higher temperatures.

There is a slight pattern in the steady-state creep data when comparing effects of temperature in Fig. 6. Results show there is a general increase in rate as temperature increases, with some blemishes in the trend. An increase in creep rate is expected with increasing temperature, as some softening is expected, and creep generally increases at higher temperatures. The noise at higher temperatures is due to higher air convection. Despite the noise, the general trend is still visible. Because we cannot compare the average of several creep tests, it is difficult to determine the error. Changes in steady-state creep rates with respect to temperature and aging will become more apparent above the glass transition

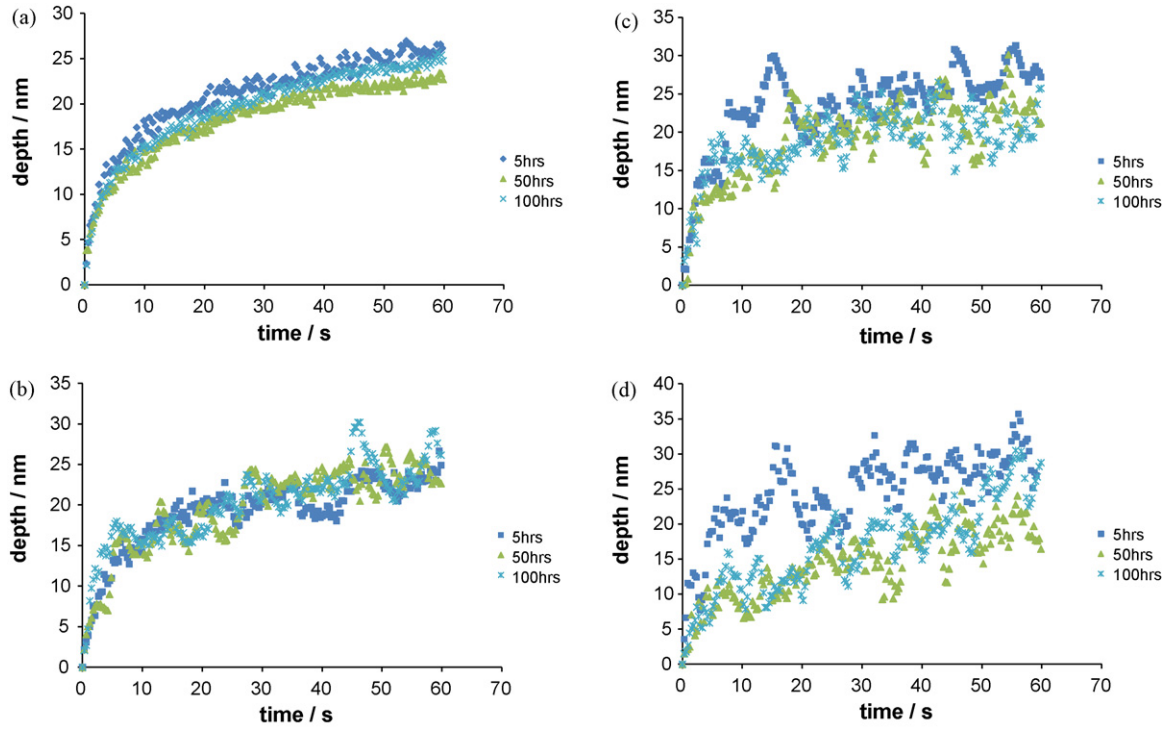

Fig. 5. Creeps tests done for samples aged different amounts of time at (a) room temperature, (b) 200 °C, (c) 300 °C, and (d) 400 °C.

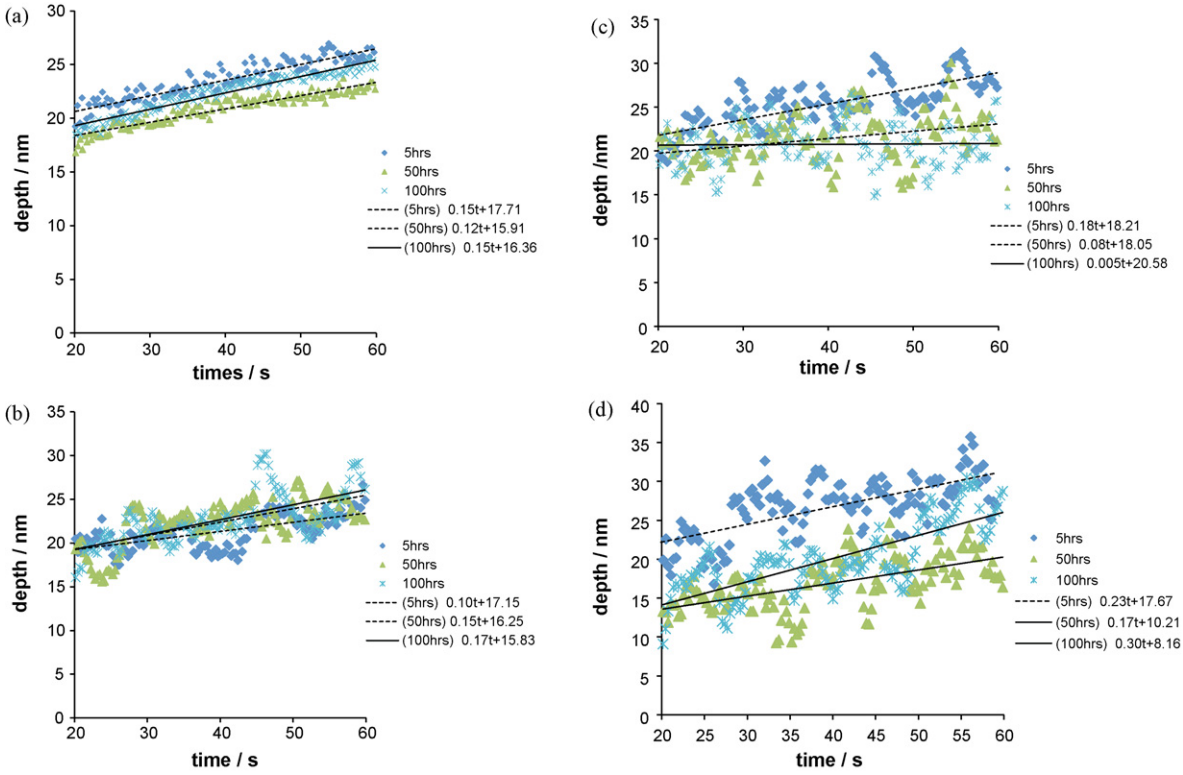

Fig. 6. Steady-state creep at (a) room temperature, (b) 200 °C, (c) 300 °C, and (d) 400 °C.

temperature, 619 °C. In general, creep becomes more measurable about T_g. As soon as facilities become available, these tests will be repeated at higher temperatures. Modeling and prediction of the creep behavior, however, can begin for temperatures below T_g.

4. Conclusions

In this study, high-temperature nanoindentation experiments were performed on G18, a glass–ceramic intended for SOFC seal use. Constant loading rates were applied during the loading segment, and a creep test was performed at maximum load for 60 s. This study focused on the plastic deformation, rather than elastic deformation, due to the indentation.

Creep tests performed at higher temperatures gave more linear results, while testing at higher temperatures gave a more logarithmic shaped creep curve. The logarithmic shaped curve is due to significant primary creep, which is usually more apparent at higher temperatures. This suggests viscoelastic effects during the loading segment at higher temperatures, and a greater creep resistance at lower temperatures. Samples with higher crystallinity were more resistant to creep.

Steady-state creep tended to increase with increasing temperature. Steady-state creep did not show a trend with respect to aging, which is more likely due to the fact that the tests were performed below the glass transition temperature. It would be highly beneficial to repeat these tests for longer creep times and at higher temperatures, past the glass transition temperature, and well into the operating temperature range.

References

[1] N. Lahl, L. Singheiser, K. Hilpert, Proc. Electrochem. Soc. (SOFC-IV) (99–19) (1999) 1057–1066.
[2] S. Yang, Y. Zhang, K. Zeng, J. Appl. Phys. 95 (2004) 3655–3666.
[3] Z. Yang, K. Meinhardt, J. Stevenson, J. Electrochem. Soc. 150 (2003) A1095–A1101.
[4] Z. Yang, J. Stevenson, K. Meinhardt, Solid State Ionics 160 (2003) 213–225.
[5] K. Weil, J. Deibler, J. Hardy, D. Kim, G. Xia, L. Chick, C. Coyle, J. Mater. Eng. Perform. 13 (2004) 316–326.
[6] E. Stephens, J. Vetrano, B. Koeppel, Y. Chou, X. Sun, M. Khaleel, J. Power Sources 193 (2009) 625–631.
[7] Z. Yang, K. Weil, D. Paxton, J. Stevenson, J. Electrochem. Soc. 150 (2003) A1188–A1201.
[8] W. Liu, X. Sun, M. Khaleel, J. Power Sources 185 (2008) 1193–1200.
[9] H. Shang, T. Rouxel, J. Am. Ceram. Soc. 88 (2005) 2625–2628.
[10] H. Shang, T. Rouxel, M. Buckley, C. Bernard, J. Mater. Res. 21 (2006) 632–638.
[11] B. Briscoe, L. Fiori, E. Pelillo, J. Phys. D Appl. Phys. 31 (1998) 2395–2405.
[12] B. Briscoe, K. Sebastian, M. Adams, J. Phys. D Appl. Phys. 27 (1994) 1156–1162.
[13] B.D. Beake, G.A. Bell, W. Brostow, W. Chonkaew, Polym. Int. 56 (2007) 773–778.
[14] B. Beake, J. Smith, Philos. Mag. A 82 (2002) 2179–2186.
[15] M. Vanlandingham, J. Villarrubia, W. Guthrie, G. Meyers, Macromol. Symp. 167 (2001) 15–43.
[16] M. Oyen, R. Cook, J. Mater. Res. 18 (2003) 139–150.
[17] B. Nguyen, B. Koeppel, S. Ahzi, M. Khaleel, P. Singh, J. Am. Ceram. Soc. 89 (2006) 1358–1368.
[18] M. Hyatt, N. Bansal, J. Mater. Sci. 31 (1996) 172–184.
[19] N. Bansal, E. Gamble, J. Power Sources 147 (2005) 107–115.
[20] W. Oliver, G. Pharr, J. Mater. Res. 7 (1992) 1564–1583.
[21] G. Pharr, W. Oliver, F. Brotzen, J. Mater. Res. 7 (1992) 613–617.